Journal of Biomedical Optics

SPIEDigitalLibrary.org/jbo

Comparative study of protoporphyrin IX fluorescence image enhancement methods to improve an optical imaging system for oral cancer detection

Ching-Fen Jiang
Chih-Yu Wang
Chun-Ping Chiang

SPIE

Comparative study of protoporphyrin IX fluorescence image enhancement methods to improve an optical imaging system for oral cancer detection

Ching-Fen Jiang,[a] Chih-Yu Wang,[a] and Chun-Ping Chiang[b]
[a]I-Shou University, Department of Biomedical Engineering, Kaohsiung, Taiwan
[b]National Taiwan University Hospital, Department of Dentistry, Taipei, Taiwan

Abstract. Optoelectronics techniques to induce protoporphyrin IX fluorescence with topically applied 5-aminolevulinic acid on the oral mucosa have been developed to noninvasively detect oral cancer. Fluorescence imaging enables wide-area screening for oral premalignancy, but the lack of an adequate fluorescence enhancement method restricts the clinical imaging application of these techniques. This study aimed to develop a reliable fluorescence enhancement method to improve PpIX fluorescence imaging systems for oral cancer detection. Three contrast features, red-green-blue reflectance difference, R/B ratio, and R/G ratio, were developed first based on the optical properties of the fluorescence images. A comparative study was then carried out with one negative control and four biopsy confirmed clinical cases to validate the optimal image processing method for the detection of the distribution of malignancy. The results showed the superiority of the R/G ratio in terms of yielding a better contrast between normal and neoplastic tissue, and this method was less prone to errors in detection. Quantitative comparison with the clinical diagnoses in the four neoplastic cases showed that the regions of premalignancy obtained using the proposed method accorded with the expert's determination, suggesting the potential clinical application of this method for the detection of oral cancer. [DOI: 10.1117/1.3595860]

Keywords: optical biopsy; oral cancer; malignancy distribution; fluorescence images; image segmentation.

Paper 10328RR received Jun. 12, 2010; revised manuscript received May 8, 2011; accepted for publication May 10, 2011; published online Jul. 8, 2011.

1 Introduction

Over the past two decades, the incidence of oral cancer has dramatically increased in many countries,[1,2] and the high prevalence has made it one of the most common malignancies in the world.[3] Oral cancer has one of the lowest five-year survival rates among the major cancers: the five-year survival rate at the fourth stage of oral cancer is less than 20%, compared with 80% for localized lesions.[4] This indicates that early detection followed by efficient treatment is one of the best ways to reduce mortality from this disease. However, accurate demarcation of early-stage neoplasia is difficult by visual inspection alone.[5–9] Clinicians can usually identify white oral leukoplakia, red oral erythroplakia, and erythroleukoplakia visually, but they cannot know which specific lesion site contains dysplastic or malignant cells. Thus, demarcation of the tumor borders via simple inspection or other common diagnostic procedures often remains unsatisfactory.

To date, biopsy remains the most reliable method for diagnosing oral cancer. However, it has limited application in detecting early-stage oral neoplastic tissue. Oral premalignant lesions such as leukoplakia, erythroplakia, and erythroleukoplakia are not homogeneous; that is, some parts of the lesion may show only hyperkeratosis and acanthosis, whereas other parts may show epithelial dysplasia, carcinoma *in situ*, or invasive carcinoma. Thus, one lesion may need multiple biopsies to avoid misdiagnosis of the most severe part of the lesion. However, biopsy is an invasive procedure and is not suitable for wide-area screening at the early stage of malignancy because the induced pain and inconvenience may seriously affect the patient's quality of life. Moreover, a plausible biopsy from an improper locus can lead to a false prognosis. Thus, determining the biopsy loci is always a dilemma and highly dependent on the clinician's experience.

In the search for a noninvasive alternative, researchers have employed modern optoelectronics techniques with light-induced fluorescence for oral cancer detection. Two types of fluorescence indicators have been reported to be valuable: autofluorescence[5,8–13] and protoporphyrin IX (PpIX) fluorescence.[6,14–18] Previous studies have shown autofluorescence to reduce with oral malignancy;[5,9,10,19,20] however, this change is not easy to discriminate by visual inspection. A study applied classification algorithms to compare various contrast features extracted from multispectral optical images and found that the ratio of red-to-green fluorescence intensity in a 405-nm excited autofluorescence image maximized the image contrast for the differentiation of neoplastic and non-neoplastic tissue.[8,10] In another study by the same authors, a computer program was developed to delineate the dysplastic area on the autofluorescence image over the white light image to increase the ability to identify the region.[21] In contrast, although 5-aminolevulinic acid (ALA) induced PpIX fluorescence has been reported to be able

Send all correspondence to: Ching-Fen Jiang, I-Shou University, Department of Biomedical Engineering, No. 1, Sec.1, Hsueh-Cheng Road, Ta-Hsu Hsiang, Kaohsiung County, Taiwan 84001; Tel: 886–7-6577711/ext. 6711; Fax: 886–7-657; E-mail: cfjiang@isu.edu.tw.

1083-3668/2011/16(7)/076006/8/$25.00 © 2011 SPIE

to overcome the limitations of autofluorescence in the differentiation between dysplasia and cancer,[17,22] the lack of comparison studies to evaluate the validity of the various image processing algorithms means that standard contrast enhancement methods are unavailable. We believe that efficient image processing methods independent of different filtering techniques can improve the insufficiencies accompanying image acquisition so that ALA-induced PpIX fluorescence imaging can be clinically applied to oral cancer detection.

Protoporphyrin IX fluorescence induced by the application of ALA is one of the most promising methods for identifying oral malignancies. However, in contrast to its high sensitivity (95 to 100%), the low specificity (50 to 60%) hinders its clinical application.[19,23] To increase the specificity of this method, various researchers have proposed that the intensity ratio may be a better indicator of malignancy than PpIX intensity alone. Scott et al.[16] and Betz et al.[19] used the red-to-green fluorescence intensity ratio and employed a commercial software package, whereas Zheng et al.[23] used the red-to-blue intensity ratio with a self-developed program for contrast-enhanced fluorescence image processing. Although their results show increased specificity by this approach, there is no consensus on the intensity ratio to be used, and the foundation of these methods was not clearly explained, hence rendering their reproducibility limited. In addition, these current methods only increase the fluorescence contrast *in situ* by mapping the original pixel values into rescaled pseudo-colors; however, determination of the location of the detected abnormal margin should refer to the corresponding white light image. This is usually a difficult task for an observer, because the positions of these two images are not exactly the same if the camera and patient are not immobilized in their relative position.

This study had two goals: first, to identify the optimal PpIX fluorescence contrast features from those categorized in previous reports and second, to fuse the detected fluorescence region with the corresponding white light image using image processing techniques for ease of identification. Thus, this method could be integrated with previously developed-fluorescence spectroscopy methods[22] to improve its clinical feasibility for oral cancer detection via wide-area inspection.

2 Methods

2.1 *Instrumentation and Image Acquisition*

An optical endoscopic system was set up for fluorescence image acquisition. The configuration of the fluorescence imaging system is shown in Fig. 1. A violet laser diode (NDHV310ACA, 30 mW, 410 nm; Nichia Co., Japan) was used as the light excitation source, which was guided into a quartz fiber bundle with a diffuse lens at the distal end. If the laser reflection is too strong, it will not only overwhelm the fluorescence but will also saturate the CCD camera, and so, a long pass filter (cutoff wavelength = 420 nm) was mounted on the camera to reduce laser reflection. The digital images, red-green-blue (RGB) bmp files with the resolution of 960 × 720 pixels, 8-bit per color channel, were captured using a color CCD camera (Sony DFW-SX900) and transferred to a notebook PC through the IEEE 1394 port for further analysis. The fundamentals of the design have been described in detail elsewhere.[11]

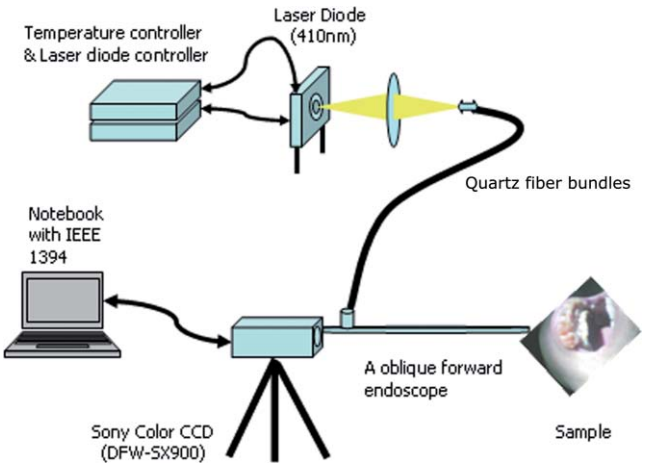

Fig. 1 Configuration of the fluorescence imaging system.

ALA was prepared according to a previous study[22] and was topically applied at a dose of 0.05 mL/cm^2 to the oral mucosa of human subjects. A pair of images was captured every half an hour from the initiation of ALA application for two hours. For each measurement, a fluorescence image was first captured under diode laser illumination and then a white-light image was acquired using a normal white-light source; this order was followed to reduce the chance that the absolute fluorescence intensity began to decrease after reaching saturation when the duration of image acquisition was prolonged. The white light image was used as the background for demarcation of the detected fluorescence so that the position could be clearly revealed. Image acquisition was performed in a dark room to avoid any interference from other light sources.

2.2 *Basis and Development of the Image Processing Method*

The basis for using ALA-induced PpIX fluorescence strength as an indicator of malignancy is that PpIX conversion is decreased in malignant tissue due to reduced ferrochelatase activity; therefore, on applying ALA (an exogenous tumor-localized fluorescent agent) to the oral mucosa, cancer cells accumulate PpIX faster than normal tissue.[20] The PpIX absorption wavelength in the human mouth is between 325 and 650 nm, and the dominant peak is at around 410 nm. Thus, if PpIX is irradiated using a diode laser with a wavelength of 410 nm, red fluorescence occurs. The fluorescence intensity in the malignant tissue reaches a maximum between 1 and 2 h after ALA application.[6,17,22,24] Numerous studies have shown that violet laser excitation induces both autofluorescence and ALA-induced fluorescence.[15,16,18–20] The wavelength of the former is in the green-to-red range, whereas that of the latter falls mainly in the red band. Although both types of fluorescence are seen in healthy and malignant tissue, autofluorescence tends to decrease and PpIX fluorescence tends to increase in malignant tissue.[19,20]

In comparison with other techniques,[16,23] in which RGB mosaic filters have been used to separate the color bands of the fluorescence image, this approach directly uses the pixel values from each color channel of the RGB images to derive the contrast features. The inherent RGB color model of the Sony camera

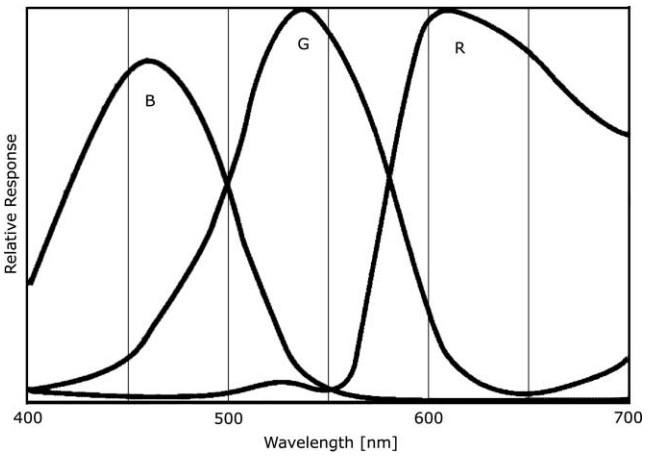

Fig. 2 Wavelength sensitivity ranges for the three color channels of the camera system.

system is leveraged to directly decompose the fluorescence images along the wavelength bands indicated in Fig. 2. The wavelength range of ALA-induced fluorescence after 410-nm illumination is 600 to 750 nm, and so, falls almost completely in the red band. The dominant peak of autofluorescence is at around 530 nm (480 to 550 nm) in the green band, while the specular and diffuse reflectance of the 410-nm violet laser falls in the blue band. This direct correspondence between the RGB wavelength sensitivity ranges and the three types of light emission (PpIX fluorescence, autofluorescence, and laser reflectance) provides a straightforward approach to measure the relative intensities.

2.2.1 *Mathematical model of PpIX fluorescence images*

To explore the contrast features, a mathematical model of the PpIX fluorescence images was built according to the corresponding optical physics of the RGB channels described above. Let $R(x,y)$, $G(x,y)$, and $B(x,y)$ represent the three primary images as functions of a pixel location (x,y) in the RGB model. Using the illumination–reflectance model, an image can be expressed by Eqs. (1)–(3), where the functions of $i(x,y,\lambda), r(x,y,\lambda), f(x,y,\lambda)$, and $CCD(\lambda)$denote the illumination, reflectance, fluorescence, and inherent RGB color transformation of the CCD camera, respectively.

$$R(x,y)=\int [i(x,y,\lambda)r(x,y,\lambda)+f(x,y,\lambda)]CCD_{\mathrm{R}}(\lambda)d\lambda, \tag{1}$$

$$G(x,y)=\int [i(x,y,\lambda)r(x,y,\lambda)+f(x,y,\lambda)]CCD_{\mathrm{G}}(\lambda)d\lambda, \tag{2}$$

$$B(x,y)=\int [i(x,y,\lambda)r(x,y,\lambda)+f(x,y,\lambda)]CCD_{\mathrm{B}}(\lambda)d\lambda. \tag{3}$$

As the violet laser was the only light source, the blue illumination should mainly contribute to the blue image, the PpIX fluorescence falls in the red band and the autofluorescence lies in the green band. Based on this argument, the three equations can be reduced to

$$R(x,y)=\int f_{PpIX}(x,y,\lambda)CCD_{\mathrm{R}}(\lambda)d\lambda=F_R, \tag{4}$$

$$G(x,y)=\int f_{auto}(x,y,\lambda)CCD_{\mathrm{G}}(\lambda)d\lambda=F_G, \tag{5}$$

$$B(x,y)=\int [i(x,y,\lambda)r(x,y,\lambda)]CCD_{\mathrm{B}}(\lambda)d\lambda=I_B. \tag{6}$$

Based on these analyses, the image processing algorithms to detect oral malignancy were developed.

2.2.2 *Extraction of contrast features*

Three contrast features commonly used to enhance the PpIX fluorescence were compared in order to find the optimum method. The theory and derivation of each of the methods are described below.

The first feature is the reflectance difference (S) between the red image (R) and the other images (G or B). This can be conducted by the binary morphological image processing technique, as

$$S=\left\{S|\bigcup \text{pixel}\in S_R\cap Not(S_G\cap S_B)\right\}, \tag{7}$$

where S_R, S_G, and S_B denote the regions with the strongest values obtained from the classification process described in the following Sec. 2.2.3 for the RGB primaries, respectively.

The second is the red-to-blue (R/B) ratio image, which can be defined as

$$R/B=\frac{\int f_{PpIX}(x,y,\lambda)CCD_R(\lambda)d\lambda}{\int i(x,y,\lambda)r(x,y,\lambda)CCD_B(\lambda)d\lambda}=\frac{F_R}{I_B}. \tag{8}$$

The third is the red-to-green (R/G) ratio image, which can be defined as

$$R/G=\frac{\int f_{PpIX}(x,y,\lambda)CCD_R(\lambda)d\lambda}{\int f_{auto}(x,y,\lambda)CCD_G(\lambda)d\lambda}=\frac{F_R}{F_G}. \tag{9}$$

The ratio values were also classified into three levels by the following classification process.

2.2.3 *Classification algorithm and image processing*

A moment-preserving algorithm[25] was used to classify the strength of each feature image into three levels. This algorithm automatically and objectively determines the intensity threshold value(s) within an image histogram that maximize(s) the variability between the resulting pixel classes; thus, it separates the image into clusters of like intensities. The one-threshold algorithm was modified into two thresholds to classify each primary image into three clusters. In the algorithm, the between-class variance σ_B^2 was calculated as thresholds k_1 and k_2 were varied

$$\boldsymbol{\sigma}_B^2(k_1,k_2)=w_0(\boldsymbol{\mu}_0-\boldsymbol{\mu}_T)^2+w_1(\boldsymbol{\mu}_1-\boldsymbol{\mu}_T)^2+w_2(\boldsymbol{\mu}_2-\boldsymbol{\mu}_T)^2, \tag{10}$$

where w_0, w_1, and w_2 are the probabilities of the three nonoverlapping classes in the images; μ_0, μ_1, and μ_2 are their mean

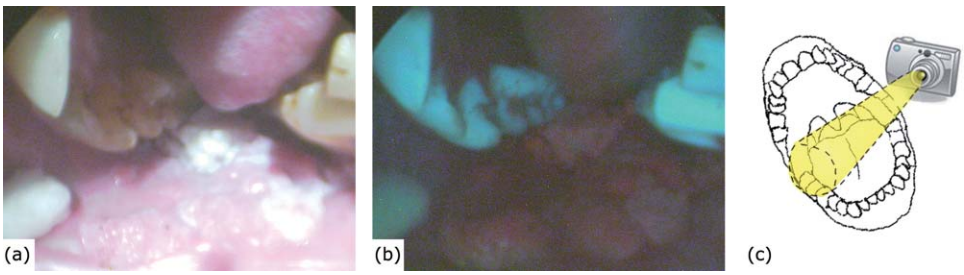

Fig. 3 (a) Original white light image and (b) corresponding fluorescence image. Both images were taken at the same site, as indicated in the graph shown in (c).

intensities; and μ_T is the mean of the entire image. The two optimal thresholds k_1^* and k_2^* are determined when σ_B^2 is maximal.

The clustering results were then pseudo-color-encoded to reveal the three relative intensity levels within an image. The pseudo-color of green was assigned to the regions with the highest level and then superimposed on the corresponding white-light image to make them easy to identify. As the fluorescence and white light images were captured in sequence, the positions of the two images could differ slightly due to patient movement. To account for this, image registration was conducted using a rigid transformation with two manually-selected reference points.

To fill the originally-detected foggy pattern of the detected region such that the region was able to be quantitatively compared with the manual demarcation, image morphological processing[26] of "opening" followed by "closing" operations was conducted using a diamond-shape structural element with a size of 5 × 5.

2.3 *Clinical Testing Method*

Five clinical cases, a normal volunteer and four patients, were then studied to evaluate the validity of the proposed methods. The normal case was used as the control. The neoplastic regions in the patients were histopathologically confirmed. The procedure of clinical examination includes initial evaluation, which was carried out by visual inspection, to determine the region covering red oral lesions with some degree of epithelial dysplasia. Following that, further verification was performed using 1% toluidine blue vital stain to stain the dysplastic and cancer cells. Finally, according to the indication by toluidine blue vital staining, the most severe part (deep-blue-stained area containing either dysplastic or cancerous cells) of the oral lesion was then selected from which to take a biopsy. The appropriate size of the biopsy specimen was about 1.0 × 0.5 × 0.8 cm (length × width × depth).

The Jaccard index (*JI*) was used to quantify the degree of the consistency between two regions. The *JI* is defined as the ratio of the intersection of two regions by the union of them. If the two regions completely overlap, the *JI* value is equal to 100%.

3 Results

3.1 *Classification*

An example image taken from the right buccal mucosa of a biopsy confirmed dysplasia case is given in Fig. 3. Classification of the RGB images of the fluorescence image shown in Fig. 3(b) is given in Fig. 4, where the three intensity levels from high to low are shown as black, pink, and white, respectively. Table 1 shows the quantitative evaluation of the mismatch in the reflection pattern between the three primaries. Both the qualitative and quantitative results reveal that the red image contains the greatest regional differences as compared with the other images across the three levels. As revealed in Fig. 4, this discrepancy can be mainly attributed to the black regions in the red image, which not only cover the teeth but also spread over the buccal mucosa and the tongue. In contrast, the black regions occur only around the teeth in the green and blue images. In addition, the lesser pink distribution in the green image, as shown in Fig. 4(b), indicates that the decrease in autofluorescence weakens the overall intensity strength in the green image as compared with that in the blue image shown in Fig. 4(c). Such regional differences in the classified patterns between the red and the other primary images show the location in which the strongest PpIX fluorescence occurs and thus reveal the malignant soft-tissue regions.

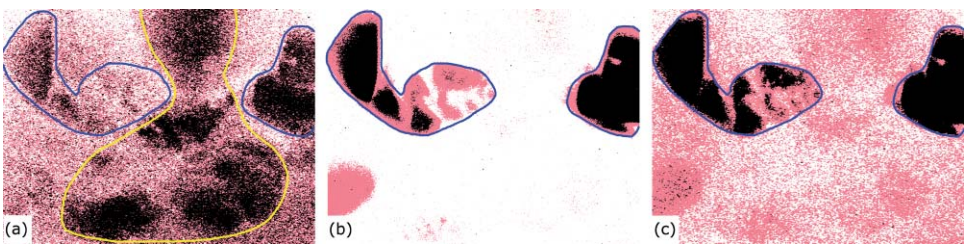

Fig. 4 Clustering results reveal different reflectance patterns of the fluorescence image shown in Fig. 3(b). The region of PpIX fluorescence (highlighted by the yellow contour) is only revealed in the red primary image shown in (a), while strong reflectance from the teeth (highlighted by the blue contour) is shown not only in the red but also in (b) the green and (c) the blue image. The extracted fluorescence region enables possible demarcation of dysplasia. (Color online only.)

Fig. 5 Comparison of the detection of dysplasia using contrast features of (a) S, (b) R/B, and (c) R/G.

3.2 *Comparison of Contrast Features*

According to the above analysis of the different classification results of the RGB primary images, the three contrast features, i.e., S, R/B, and R/G, were derived and their performance was compared.

Following rigorous comparison, the R/B ratio images were found to be invalid in terms of enhancement of the contrast between neoplastic and non-neoplastic tissue in all cases. The example shown in Fig. 5 demonstrates sparsely-dispersed black dots in the R/B ratio image in contrast to the dense black dots concentrated in the dysplastic regions in the S and R/G images. The low contrast in the R/B ratio was further confirmed by the long-tailed pattern of the histogram of the R/B ratio images (Fig. 6), indicating small amounts of pixels belonging to the third level. In comparison, the histogram of the R/G values shows a clear clustered pattern. Both results demonstrate the inability to use R/B as a contrast feature to extract the neoplastic regions.

After weeding out the R/B feature, the contrast features of the reflectance difference (S) and the R/G ratio were further compared to inspect the detected locations in terms of the originally-detected foggy patterns spatially registered with the corresponding white light image. Figure 7 demonstrates the results of the negative control case with a fully normal image and the case with neoplastic regions. In the control case, the green dots are few in number and are randomly scattered on the healthy mucosa in the R/G image, whereas denser dots are spread not only on the mucosa but also on the white glove in the S image. In the neoplastic case, even though both methods detected neoplasia, the feature S tended to result in false detection at the two white cotton swabs, where strong reflection occurs. Table 2 lists the differences in the green dot density between the three regions.

Table 1 *JI* values from the fluorescence images.

	Primary image pair		
Region	Red versus Green	Red versus Blue	Green versus Blue
black	16.86%	17.24%	69.47%
pink	11.84%	30.08%	13.52%
white	24.18%	24.08%	47.83%

3.3 *Consistency in Detection*

The consistency in the detected location is demonstrated in Figs. 8(a) and 8(b). These two images were taken from the same region of the same patient by rotating the camera about 30 degrees counter-clockwise, and the distribution of detection shown as green dots on both images still remains localized in the same malignant region – the right buccal mucosa.

3.4 *Comparison with Expert Delineation*

Through comparative study, the R/G ratio was selected as the optimal contrast enhancement method. To verify its reliability, detection using the R/G ratio image was further compared with the results obtained by clinical examination in four neoplastic cases. This was accomplished by overlapping the detected regions and the manual delineation by an experienced dentist according to the clinical examination, as shown in Fig. 9. The degree of correspondence between them was quantitatively evaluated by the *JI*, as indicated in the caption of Fig. 9.

In order to identify the grade of severity of the pathology, the pseudo-color of a pixel is defined as an exponential function of its *R/G* value. As the original fused images (Fig. 7) only revealed the detected area, the grade of severity was unclear in such images. Therefore, the color of the detected area was scaled into the color range according to the absolute value of *R/G* in the final registered image to provide more information for diagnosis. As the value increased, the color tended to be more reddish, as demonstrated in Fig. 9. It can be seen that cases 1 and 2, with fibrosis only, revealed a green color and cases 3 and 4, with dysplasia, turned to yellow, and their most severe parts (deep yellow) fell inside the manually delineated areas. The results shown in Fig. 9 indicate that the neoplastic sites detected by this method accorded with the clinical diagnosis.

4 Discussion

Optoelectronics techniques with light-induced fluorescence have been proposed as noninvasive alternatives to conventional

Table 2 Dot densities measured in the three regions labeled in Fig. 6.

Dot density	Cotton swab	Neoplastic tissue	Normal tissue
Fig. 6(b)	**97.8%**	**91.7%**	**22.6%**
Fig. 6(d)	**0%**	**76.2%**	**11.9%**

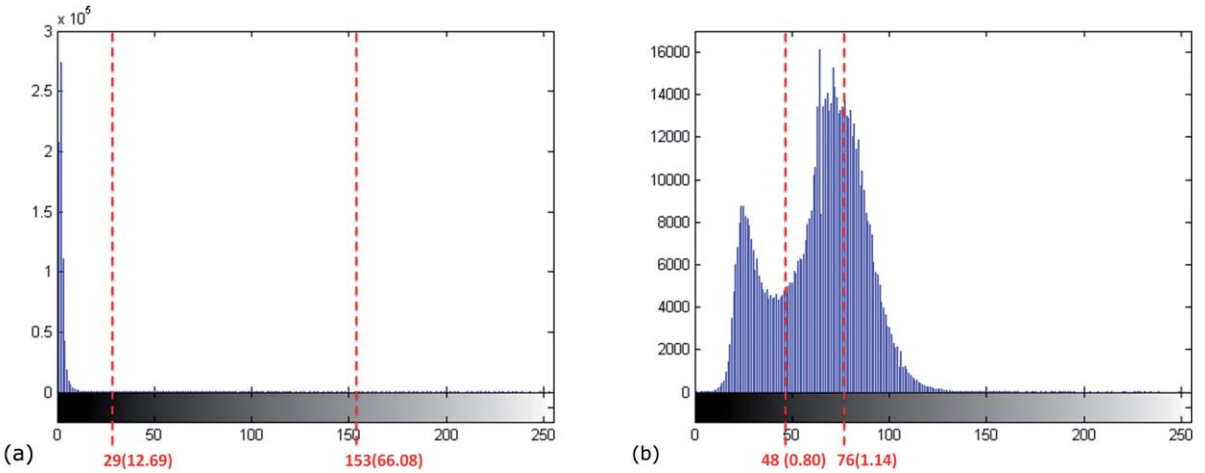

Fig. 6 Normalized histogram of the (a) R/B and (b) R/G ratio images. The two optimal normalized thresholds values are indicated by red lines in each histogram. The original ratio values were normalized to be within the visible image intensity range. The corresponding original thresholds are given in parentheses. (Color online only.)

biopsy to detect oral cancer in the early stages of malignancy. Spectroscopic studies have reported that ALA induced-PpIX fluorescence is a promising method to improve the detection of premalignant lesions on oral fibrotic mucosa that cannot be found by autofluorescence.[17,22] In comparison to the small field covered by a spectrofluorometer, fluorescence imaging provides a much broader area for inspection. However, unlike autofluorescence, for which the optimal contrast mechanism has been carefully verified by Roblyer et al.,[21] the contrast enhancement methods for PpIX fluorescence imaging are diverse and lacks verification. Given the absence of an adequate image processing method among current techniques, we attempted to compare common contrast features by their optical properties related to the changes in fluorescence intensity associated with premalignancy and to develop a reliable image processing method to improve PpIX fluorescence imaging systems for oral cancer detection.

The reflection patterns of the RGB primaries of the fluorescence images were first analyzed under the assumption that differences between them can be used as features to differentiate malignancy. According to arguments regarding the three spectral responses dominating in different RGB channels, as summarized in Eqs. (4)–(6), this assumption can be supported by the following findings in the classified patterns of the RGB primaries of a fluorescence image. First, the broader black distribution in the segmentation of R(x,y) is mainly contributed to by PpIX fluorescence. Second, the malignancy-related decrease in autofluorescence indicated by a reduced contrast in G(x,y) was in agreement with other studies.[5,9,10] In addition, this difference was not observed in the same analysis of the corresponding white light image in our pilot study.[27]

After verification of this assumption, three contrast features, the RGB reflectance difference, the R/B ratio, and the R/G ratio, were derived based on the optic characteristics drawn from the analysis. A comparative study of five clinical cases suggested that the R/G ratio provides the greatest image contrast between oral dysplastic and nondysplastic tissue. The advantage of the R/G ratio over the reflectance difference S can be explained by inspecting the illumination–reflectance model of Eqs. (1)–(3) and the wavelength sensitivity ranges of the camera system shown in Fig. 2. In the control case, in which PpIX fluorescence

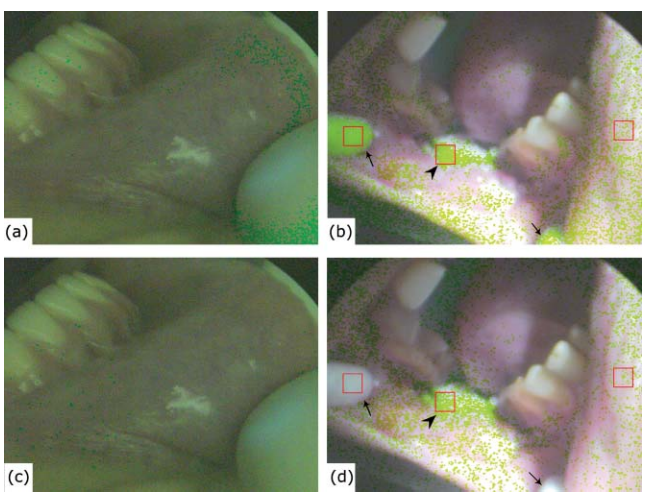

Fig. 7 (a) and (c) Original foggy-patterns detected using S and R/G features of the negative control; (b) and (d) the neoplastic case. The arrows indicate two cotton swabs and the arrow head indicates the neoplastic lesion. Three boxes of a size of 120 × 120 were used to measure the green point density, as listed in Table 2; these are located on the cotton swab, the neoplastic lesion, and the normal mucosa, from left to right.

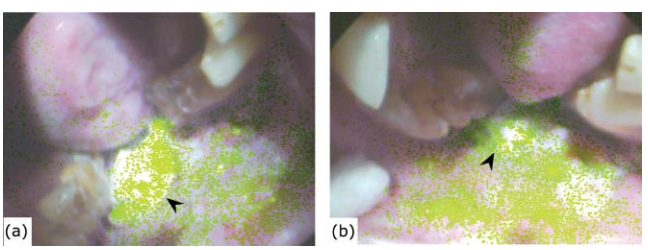

Fig. 8 Regions of neoplasia (arrow-heads) are consistently detected when the camera was rotated counter-clockwise about 30 deg from (a) to (b).

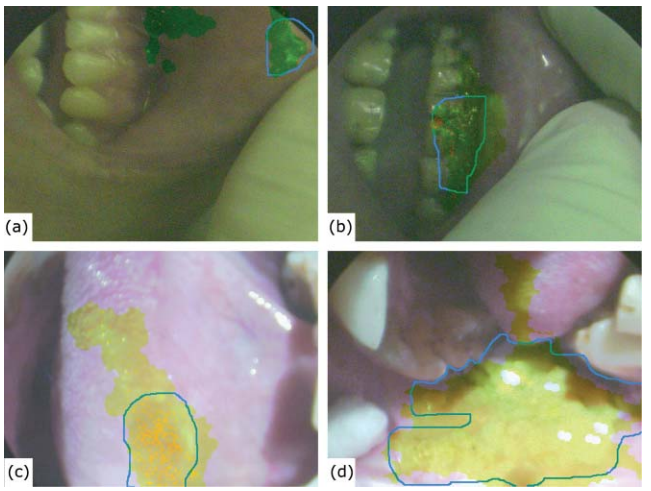

Fig. 9 Demarcations detected in the four cases overlapping the corresponding manual delineations (represented as blue contours) by an experienced dentist according to the histopathological results. (a) Fibrosis, $JI = 37.56\%$; (b) hyperplasia, $JI = 52.64\%$; (c) dysplasia, $JI = 63.06\%$; and (d) dysplasia, $JI = 82.02\%$. (Color online only.)

is absent, the red intensity, R(x,y), is mainly contributed to by the laser reflectance. In the neoplastic case, with white cotton swabs where strong laser reflection occurs, R(x,y) is equally contributed to by the laser reflectance and the fluorescence. In such a case, the classification of R(x,y) does not reflect the strength of fluorescence alone. Thus, the feature S, based on extracting the distributional difference in R(x,y) from the other images, is prone to error detection. In contrast, false classification can be avoided in the R/G ratio in both cases because the factor of laser reflectance is canceled out through normalization. Therefore, the ratio image of R/G results in more accurate detection without the interference of illumination.

The reason for the superiority of the R/G contrast features over the R/B values is also discussed herein. In a comparison of the R/G with the R/B features, as the malignant regions are characterized by higher f_{PpIX} and lower f_{auto}, the R/G ratios should increase with the appearance of PpIX fluorescence in the malignant regions; therefore, the differences between the malignant and normal regions are amplified. In contrast, the value of R/B can be interpreted as the red fluorescence f_{PpIX} normalized by reflection of major illumination, I_B; therefore, the contrast enhancement effect is not as good as that observed for the R/G ratio.

As the R/G ratio was found to be the best contrast features by rigorous comparison, its ability to identify the regions of interest was further improved by a series of image processing methods involving classification, morphologic operation, and image registration. In comparison with the conventional ratio images that only enhance the fluorescence contrast by mapping the fluorescence image into scaled-pseudo colors, the novelties of the improved R/G ratio images are described as follows. The possibility of premalignancy was revealed in terms of a dense group of green points, which were classified as the high-contrast R/G values using a dynamic thresholding mechanism. The spatial distribution of the neoplasia was directly revealed on the white-light image, with the color as a function of the absolute R/G values such that relative spatial information of the malignancy distribution is clearly delineated in the oral cavity.

The limitations of this study are twofold. First, pathologic grading was not evaluated due to insufficient image collection. A limitation of autofluorescence in differentiating the different degrees of dysplasia to cancer is that it has been found to be affected by variation in collagen content,[10,22] and the ALA-induced PpIX method is a potential alternative to improve this inefficiency of autofluorescence. Even though this study showed a tendency toward increased R/G values associated with a more severe degree of premalignancy, more rigorous evaluation of a greater number of pathological cases needs to be carried out. Second, whether system detection or manual delineation was more accurate was not evaluated. As the imaging method enabled a wide-area screening of the mouth, while a biopsy was taken from the characteristic part with a size of no larger than 1 cm^2, it was difficult to verify the nonoverlapping areas demarcated by the system and the expert. As mentioned in Sec. 1, there are limitations in the differentiation of dysplastic or malignant lesions from non-neoplastic regions such as inflammation, hyperplasia, and hyperkeratosis simply by visual inspection. These confounding regions can be precursor margins of neoplasia and are difficult to discriminate by visual inspection; however, a significant R/G contrast is observed in these areas. This discrepancy can be further investigated in future studies. An additional note on the classification process: this was conducted separately based on the primary intensity of the RGB, R/B, and R/G values. Roblyer et al.[10] proposed a classification method using combined features to maximize the autofluorescence contrast to discriminate oral neoplasia. This classification algorithm may be further compared with the method using combined contrast features in future studies.

The study presented herein demonstrates the superiority of the R/G ratio as a contrast feature to objectively identify neoplastic and non-neoplastic oral tissue *in vivo*. In addition, image processing techniques were applied to enhance the visibility of the detected neoplastic distribution in the fluorescence images on the corresponding regions in the white images. These advantages lead us to believe that the proposed fluorescence image processing method is of great potential in terms of improving the feasibility of conventional PpIX fluorescence imaging systems as a noninvasive diagnosis modality to assist clinicians in the overall examination of the oral cavity, thereby increasing the accuracy of the diagnosis and prognosis of oral cancer.

Acknowledgments

This research was supported by the National Science Council of Taiwan (Grant Nos. NSC 92-2218-E-214-003 and NSC 91-2218-E-214-021). The authors gratefully acknowledge the expert assistance of Dr. C. T. Chen of the Center for Optoelectronic Biomedicine, National Taiwan University, in the application of ALA in this study.

References

1. D. M. Parkin, E. Laara, and C. S. Muir, "Estimates of the worldwide frequency of sixteen major cancers in 1980," *Int. J. Cancer* **41**(2), 184–197 (1988).
2. D. M. Parkin, P. Pisani, and J. Ferlay, "Estimates of the worldwide incidence of 25 major cancers in 1990," *Int. J. Cancer* **80**(6), 827–841 (1999).

3. R. Sankaranarayanan, E. Masuyer, R. Swaminathan, J. Ferlay, and S. Whelan, "Head and neck cancer: a global perspective on epidemiology and prognosis," *Anticancer Res.* **18**(6B), 4779–4786 (1998).
4. J. J. Sciubba, "Oral cancer: the importance of early diagnosis and treatment," *Clin. Dermatol.* **2**(4), 239–251 (2001).
5. P. M. Lane, T. Gilhuly, P. Whitehead, H. Zeng, C. F. Poh, S. Ng, P. M. Williams, L. Zhang, M. P. Rosin, and C. E. MacAulay, "Simple device for the direct visualization of oral-cavity tissue fluorescence," *J. Biomed. Opt.* **11**, 024006 (2006).
6. A. Leunig, K. Rick, H. Stepp, R. Gutmann, G. Alwin, R. Baumgartner, and J. Feyh, "Fluorescence imaging and spectroscopy of 5-aminolevulinic acid induced protoporphyrin IX for the dectection of neoplastic lesions in the oral cavity," *Am. J. Surg.* **172**(6), 674–677 (1996).
7. M. W. Lingen, J. R. Kalmar, T. Karrison, and P. M. Speight, "Critical evaluation of diagnostic aids for the detection of oral cancer," *Oral Oncol.* **44**(1), 10–22 (2008).
8. M. S. Rahman, N. Ingole, D. Roblyer, V. Stepanek, R. Richards-Kortum, A. Gillenwater, S. Shastri, and P. Chaturvedi, "Evaluation of a low-cost, portable imaging system for early detection of oral cancer," *Head & Neck Oncology* **2**(1), 1–8 (2010).
9. E. Svistun, R. Alizadeh Naderi, A. El Naggar, R. Jacob, A. Gillenwater, and R. Richards Kortum, "Vision enhancement system for detection of oral cavity neoplasia based on autofluorescence," *Head Neck* **26**(3), 205–215 (2004).
10. D. Roblyer, C. Kurachi, V. Stepanek, R. A. Schwarz, M. D. Williams, A. K. El-Naggar, J. J. Lee, A. M. Gillenwater, and R. Richards-Kortum, "Comparison of multispectral wide-field optical imaging modalities to maximize image contrast for objective discrimination of oral neoplasia," *J. Biomed. Opt.* **15**(6), 066017 (2010).
11. C. Y. Wang, T. Tsai, C. T. Chen, C. F. Chiang, H. M. Chen, and C. P. Chiang, "A fluorescence imaging system for oral cancer and precancer detection," in *Proc. IEEE EMBS Asian-Pacific Conf. on Biomedical Engineering*, pp. 152–153, (2003).
12. C. Y. Wang, T. Tsai, H. M. Chen, C. T. Chen, and C. P. Chiang, "PLS-ANN based classification model for oral submucous fibrosis and oral carcinogenesis," *Lasers Surg. Med.* **32**(4), 318–326 (2003).
13. Y. Wu and J. Y. Qu, "Autofluorescence spectroscopy of epithelial tissues," *J. Biomed. Opt.* **11**, 054023 (2006).
14. A. Leunig, C. S. Betz, M. Mehlmann, H. Stepp, S. Arbogast, G. Grevers, and R. Baumgartner, "Detection of squamous cell carcinoma of the oral cavity by imaging 5 aminolevulinic acid induced protoporphyrin IX fluorescence," *Laryngoscope* **110**(1), 78–83 (2000).
15. A. Leunig, M. Mehlmann, C. Betz, H. Stepp, S. Arbogast, G. Grevers, and R. Baumgartner, "Fluorescence staining of oral cancer using a topical application of 5-aminolevulinic acid: fluorescence microscopic studies," *J. Photochem. Photobiol., B* **60**(1), 44–49 (2001).
16. M. Scott, C. Hopper, A. Sahota, R. Springett, B. McIlroy, S. Bown, and A. MacRobert, "Fluorescence photodiagnostics and photobleaching studies of cancerous lesions using ratio imaging and spectroscopic techniques," *Lasers Med. Sci.* **15**(1), 63–72 (2000).
17. A. Sharwani, W. Jerjes, V. Salih, A. MacRobert, M. El-Maaytah, H. Khalil, and C. Hopper, "Fluorescence spectroscopy combined with 5-aminolevulinic acid-induced protoporphyrin IX fluorescence in detecting oral premalignancy," *J. Photochem. Photobiol., B* **83**(1), 27–33 (2006).
18. M. Suhr, C. Hopper, L. Jones, J. George, S. Bown, and A. MacRobert, "Optical biopsy systems for the diagnosis and monitoring of superficial cancer and precancer," *Int. J. Oral Maxillofac. Surg.* **29**(6), 453–457 (2000).
19. C. S. Betz, H. Stepp, P. Janda, S. Arbogast, G. Grevers, R. Baumgartner, and A. Leunig, "A comparative study of normal inspection, autofluorescence and 5 ALA induced PPIX fluorescence for oral cancer diagnosis," *Int. J. Cancer* **97**(2), 245–252 (2002).
20. B. Swinson, W. Jerjes, M. El-Maaytah, P. Norris, and C. Hopper, "Optical techniques in diagnosis of head and neck malignancy," *Oral Oncol.* **42**(3), 221–228 (2006).
21. D. Roblyer, C. Kurachi, V. Stepanek, M. D. Williams, A. K. El-Naggar, J. J. Lee, A. M. Gillenwater, and R. Richards-Kortum, "Objective detection and delineation of oral neoplasia using autofluorescence imaging," *Cancer Prevention Research* **2**(5), 423 (2009).
22. C. Y. Wang, T. Tsai, C. P. Chiang, H. M. Chen, and C. T. Chen, "Improved diagnosis of oral premalignant lesions in submucous fibrosis patients with 5-aminolevulinic acid induced PpIX fluorescence,"*J. Biomed. Opt.* **14**, 044026 (2009).
23. W. Zheng, K. C. Soo, R. Sivanandan, and M. Olivo, "Detection of neoplasms in the oral cavity by digitized endoscopic imaging of 5-aminolevulinic acid-induced protoporphyrin IX fluorescence," *Int. J. Oncol.* **21**(4), 763–768 (2002).
24. H. M. Chen, C. H. Yu, P. C. Tu, C. Y. Yeh, T. Tsai, and C. P. Chiang, "Successful treatment of oral verrucous hyperplasia and oral leukoplakia with topical 5 aminolevulinic acid mediated photodynamic therapy," *Lasers Surg. Med.* **37**(2), 114–122 (2005).
25. N. Otsu, "A threshold selection method from gray-level histograms," *Automatica* **11**, 285–296 (1975).
26. R. C. Gonzalez and R. E. Woods, "Morphological image processing," Chapter 9 in *Digital Image Processing*, 2nd ed., pp. 519–547, Prentice-Hall, Englewood Cliffs, NJ (2002).
27. C. F. Jiang, C. Y. Wang, and C. P. Chiang, "Oral cancer detection in fluorescent image by color image fusion," *Conf. Proc. IEEE Eng. Med. Biol. Soc.* vol. 1, pp. 1260–1262 (2004).